Graphite Nodule and Eutectic Cell Count in Cast Iron: Theoretical Model Based on Weibull Statistics and Experimental Verification

E. FRAŚ, K. WIENCEK, M. GÓRNY, and H.F. LÓPEZ

In this work, a model is proposed for heterogeneous nucleation on substrates whose size distribution can be described by the Weibull statistics. It is found that the nuclei density, N_{nuc} can be given in terms of the maximum undercooling, ΔT_m, by $N_{nuc} = N_s \exp(-b/\Delta T_m)$, where N_s is the density of nucleation sites in the melt and b is the nucleation coefficient ($b > 0$). When nucleation occurs on all possible substrates, the graphite nodule density, $N_{V,n}$, or eutectic cell density, N_V, after solidification equals N_s. In this work, measurements of $N_{V,n}$ and N_V values were carried out on experimental nodular and flake graphite iron castings processed under various inoculation conditions. The volumetric nodule $N_{V,n}$ or graphite eutectic cell N_V count was estimated from the area nodule count, $N_{A,n}$, or eutectic cell count, N_A, on polished cast iron surface sections by stereological means. In addition, maximum undercoolings, ΔT_m, were measured using thermal analysis. The experimental outcome indicates that the $N_{V,n}$ or N_V count can be properly described by the proposed expression $N_{V,n} = N_V = N_s \exp(-b/\Delta T_m)$. Moreover, the N_s and b values were experimentally determined. In particular, the proposed model suggests that the size distribution of nucleation sites is exponential in nature.

I. INTRODUCTION

FLAKE graphite cast iron is the most frequently used in foundry practice. Hence, there are numerous reports related to the production of cast iron, some of which are of essential importance as they are linked to the solidification of graphite eutectic. In flake graphite cast iron, the austenite-graphite eutectic solidification process is concomitant with the formation of eutectic cells that are more or less spherical (Figures 1(a) and (b)). These eutectic cells consist of interconnected graphite plates surrounded by austenite. Because each eutectic cell is the product of a graphite nucleation event, cell count measurements can be used to establish the graphite nucleation susceptibility of a given cast iron. In general, increasing the eutectic cell count in a given cast iron leads to the following:

(1) increasing strength of cast iron (through a reduction in ferrite and an increase in graphite type A);[1]
(2) reducing the chill of cast iron[2] and, as a consequence, the making of possible production machinable castings, free from the high hardness carbide eutectic;
(3) increasing preshrinkage expansion[3,4]—if the mold lacks sufficient rigidity, expansion of the

casting during solidification can cause unsoundness in the form of internal porosity or surface sinking defects, particularly in those parts of the casting last to solidify (the probability of developing unsoundness increases with the cell count).

Ductile cast iron is a modern engineering material whose production is continually increasing. In this cast iron, each nucleus of graphite gives rise to a single graphite nodule (Figure 1(d)); thus, nucleation establishes the final nodule count. Increasing the nodule count in a given ductile cast iron leads to the following:

(1) increasing strength and ductility in ADI iron,[5]
(2) reducing microsegregation of alloying elements[6,7] and improving microstructural homogeneity (here, the type of eutectic transformation, stable or metastable, is also influenced due to the redistribution of alloying elements);
(3) reducing the chilling tendency of cast iron;[8,9]
(4) increasing preshrinkage expansion;[3] and
(5) increasing the fraction of ferrite in the microstructure.[10]

Accordingly, it can be stated that graphite eutectic cell and nodule count influenced some important factors for foundry practice.

It is well known that the nodule count in ductile iron or eutectic cell count in flake graphite cast iron can be significantly influenced by the cooling rates,[1,11–13] chemical composition,[1,11–13] and bath superheat temperature and time.[12] Nevertheless, a drastic increase in

E. FRAŚ, Professor and Head, K. WIENCEK and M. GÓRNY, Assistant Professor, are with the AGH University of Science and Technology, Mickiewicza 30, Cracow, Poland. Contact e-mail: edfras@agh.edu.pl H.F. LÓPEZ, Professor and Chair, is with the University of Wisconsin–Milwaukee, Milwaukee, WI 53201, USA.
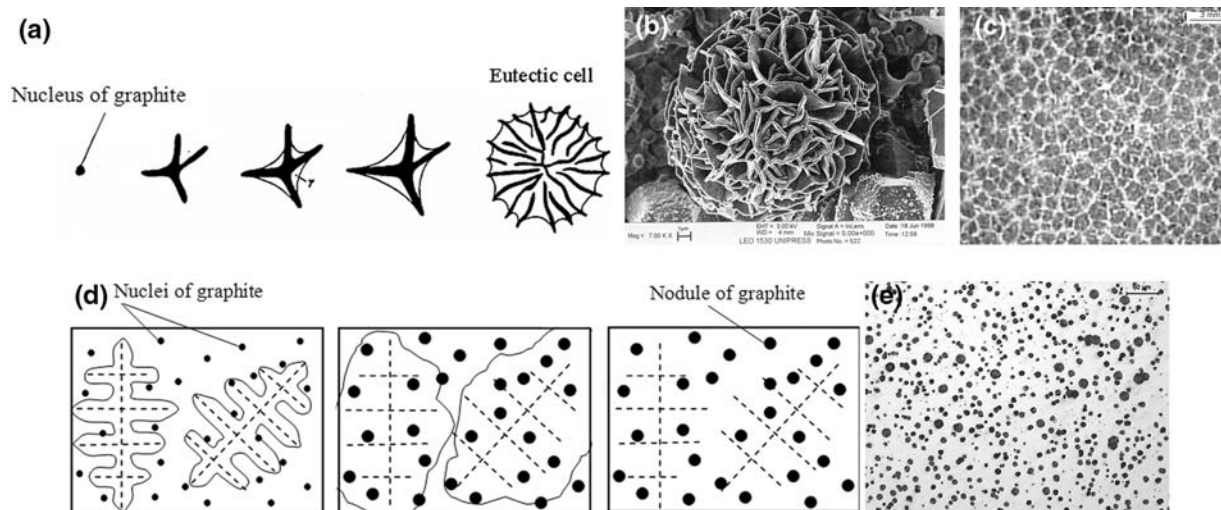
Fig. 1—Illustration of (*a*) the development of eutectic graphite-austenite cells during solidification of flake graphite cast iron; (*b*) eutectic cell; (*c*) graphite eutectic cell boundaries, etched with Stead reagent; (*d*) graphic depiction of solidification of nodular cast iron; and (*e*) structure of nodular cast iron.

the nodule or cell count is usually achieved by introducing inoculation processes.[1,11–13] Under these conditions, the exhibited graphite nodule or cell count depends on the type of inoculant,[1,12–15] quantity and granulation,[12] superheat temperature for the base metal,[12] inoculation temperature,[12] and time after inoculation.[1,12–14]

With the development of computer simulation techniques, solidification modeling has been increasingly used in the predictions of solidification microstructures.[16,17]

Accordingly, it is important to have a clear understanding of the active nucleation mechanisms and of the proper factors, which define the nucleation stage. In the published literature, the volumetric eutectic cell count N_V (number of cells per unit volume of metal) and volumetric nodule count $N_{V,n}$ (number of graphite nodule per unit volume of metal) are often related to the maximum undercooling ΔT_m, by empirical expressions of the type[18,19,20]

$$N_V = \psi (\Delta T_m)^k \qquad [1]$$

$$N_{V,n} = \sum_{i=0}^{3} \alpha_i (\Delta T_m)^i \qquad [2]$$

where ψ, α_i, k, and $i = 0, 1, 2, 3$ are experimentally determined nucleation constants. Because these equations are obtained from fitting experimental data, they do not have a definite physical meaning, even though they have been widely used.[18–21] Hence, the aim of the present work is to propose a simple analytical model for heterogeneous nucleation. In the proposed model, expressions are derived as a function of ΔT_m, which are qualitatively similar to Eqs. [1] and [2]; however, the nucleation constants have a plausible physical interpretation.

II. THEORETICAL MODEL

Nucleation is the predominant process at the onset of solidification of a molten metal and affecting significantly the final microstructure of cast iron. Assuming that each nucleus of graphite gives rise to a single nodule of graphite or eutectic cell, the expected volumetric nodule count, $N_{V,n}$, or volumetric cell count, N_V, can be described by the nuclei count, N_{nuc} (number of graphite nuclei per unit volume of liquid metal) as

$$N_{V,n} = N_V = N_{nuc} \qquad [3]$$

In liquid melts, particle-nucleation substrates of various sizes are in continuous permanent movement and mutually interacting. In turn, processes such as chemical reactions, coagulation, coalescence, and flotation at increasing times affect the number and size of the substrates. As a consequence, the number and size of substrates changes with time. In a more detailed analysis, the substrates can be characterized by a unimodal size distribution function. The substrate size distribution can then be considered as a quantitative feature of the undercooled melt, which determines the nucleation potential during solidification. Based on these arguments, a simple heterogeneous model for the nucleation on substrate surface (nucleation sites) is developed. The set of sites that are randomly distributed in the space (undercooled melt) is characterized by density N_s, which gives the number of sites per unit volume. Also, the site size, l, can be described by a continuous random variable of a Weibull distribution with the probability density given by[22]

$$f(l) = nal^{n-1} \exp(-al^n) \text{ for } l \geq 0 \qquad [4]$$

where n is a positive integer. For a given n and an average site size l_a, the parameter a can be written as

$$a = \left[\frac{\Gamma(1 + n^{-1})}{l_a}\right]^n \qquad [5]$$

where Γ is the second-order Euler function. Moreover, N_s and $f(l)$ can be related to each other through the function $\Lambda(l)$ as

$$\Lambda(l) = N_s \, f(l) \qquad [6]$$

The function $\Lambda(l)$ describes the amount and size of sites for a differential size interval $(l, l + dl)$, and it can be regarded as a quantitative feature of the state of the undercooled melt.

Accordingly, the density of nucleation sites (number of nucleation sites per unit volume of liquid metal) can be found by integrating $\Lambda(l)$ as

$$N_s = \int_0^\infty \Lambda(l)dl \qquad [7]$$

Notice that $\Lambda(l)$ depends on the function $f(l)$ (Eq. [4]) and, in particular, that for $n = 1$, $\Lambda(l)$ becomes a monotonically decreasing function, while for $n > 1$, it becomes unimodal and positively skewed (Figure 2). The proposed nucleation model for heterogeneous nucleation of a solid in an undercooled liquid is described by the function $\Lambda(l)$, which includes the Weibull distribution (Eq. [4]). Moreover, $\Lambda(l)$ is simple and flexible in the sense that it depends on two parameters (a and n) and it is very appropriate from an analytical point of view. Because not all of the set of sites take an active role in the nucleation process, the minimum site size, l_m, for a given undercooling, ΔT, from which a nucleus can grow is determined by (Figure 3)
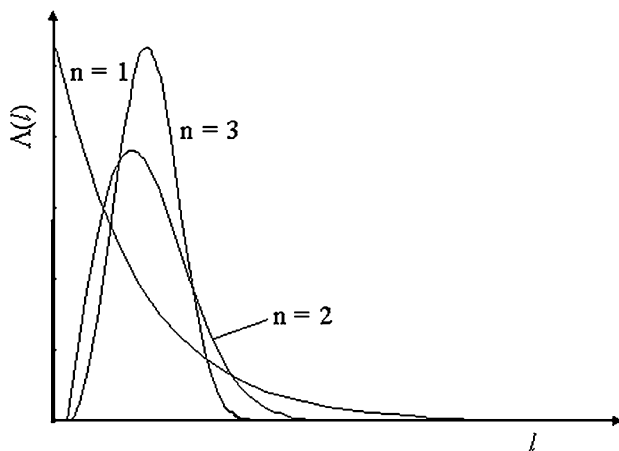
$$AB = l_m = 2r* \sin \theta \qquad [8]$$
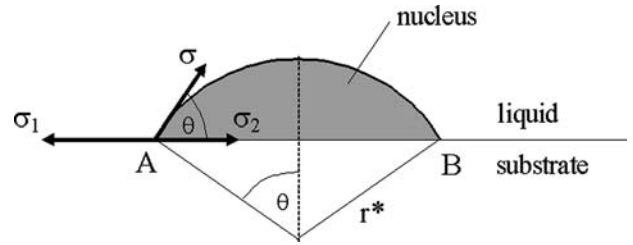
Fig. 2—Weibull distribution for $n = 1$, 2, and 3.

Fig. 3—Schematic representation of a solid nucleus on a substrate.

$$r* = \frac{2\sigma}{\Delta T \Delta S} \qquad [9]$$

where $r*$ is the critical nucleus size, θ is the wetting angle, ΔS is the entropy of solution of graphite, and σ is the nucleus-melt interfacial energy. From Eqs. [8] and [9], the minimum site size can be given by

$$l_m = \frac{\Omega}{\Delta T} \qquad [10]$$

where

$$\Omega = \frac{4\sigma \sin \theta}{\Delta S} \qquad [11]$$

Figure 4(c) shows a cooling curve where the arrows indicate the extent of undercooling at the beginning of solidification. Notice that within the time interval from t_b to t_m or undercooling from $\Delta T = 0$ to $\Delta T = \Delta T_m$, sites with sizes greater than l_m become active for nucleation (Figure 4(b)). If on all sites of sizes $l > l_m$ nuclei are formed, then at ΔT_m, which determines l_m, the nuclei density N_{nuc} can be described by

$$N_{\text{nuc}} = \int_{l_m}^\infty \Lambda(l)dl \qquad [12]$$

Substituting $\Lambda(l)$ (Eq.[6]) in Eq. [12] and using Eqs. [3] through [5] for $n = 1$ yields

$$N_{\text{nuc}} = N_{V,n} = N_V = N_s \exp\left(-\frac{b}{\Delta T_m}\right) \qquad [13]$$

where b is the nucleation coefficient given by

$$b = \frac{\Omega}{l_a} \qquad [14]$$

From Eq. [13], N_{nuc} is an increasing function of ΔT_m. The function depends on two parameters, N_s and b, whose physical meanings have been established in Eqs. [7], [11], and [14], respectively. In addition, notice that the qualitative properties of the function given by Eq. [13] are similar to those described by the empirical Eqs. [1] and [2].

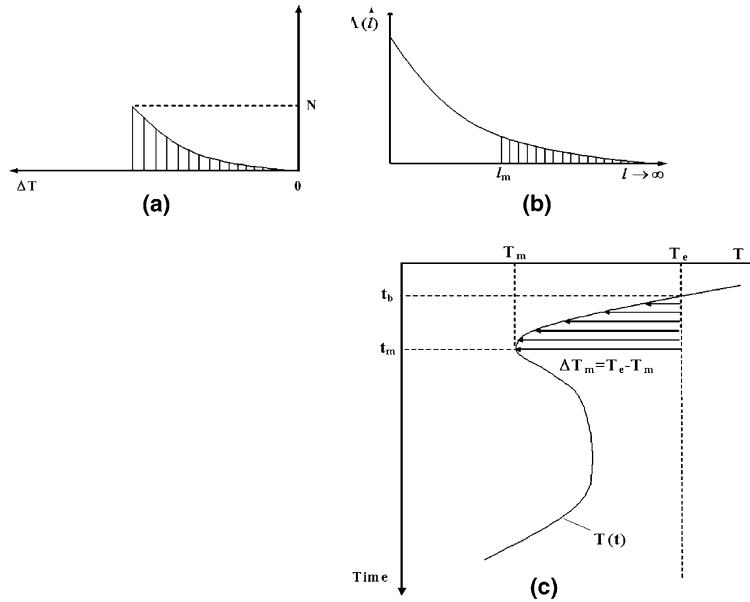Moreover, substituting Eq. [5] into Eq. [4] for $n = 1$ yields

Fig. 4—(a) Nuclei density, (b) site Weibull distribution, and (c) cooling curve.

$$f(l) = \frac{1}{l_a} \exp\left(\frac{l}{l_a}\right) \text{ for } l \geq 0 \qquad [15]$$

The preceding expression indicates that the site-size distribution in liquid metal is of exponential nature.

Notice that all of the sites from a given set of sites become active ($N_s \rightarrow N_{nuc}$) when $\Delta T \rightarrow \infty$ or $b \rightarrow 0$ (Eq. [13]). In the first case, from Eqs. [9] and [10], $r^* \rightarrow 0$ and $l_m \rightarrow 0$, whereas in the second case, $\theta \rightarrow 0$, and in accordance with Eqs. [10], [11], and [14], $l_m \rightarrow 0$, $\Omega \rightarrow 0$, and $b \rightarrow 0$. In both cases, this behavior indicates that increasingly smaller sites become active (Figure 4) from a given set of sites.

With regard to the modeling of interfaces, the crystal-melt surface energy, σ, can be described by[23]

$$\sigma = \gamma T_e \Delta S \left(\frac{V_m}{N_{Avo}}\right)^{1/3} \qquad [16][16]$$

where $\gamma = 0.86$ for fcc and hcp crystals, T_e is the equilibrium temperature of solidification, V_m is the molar
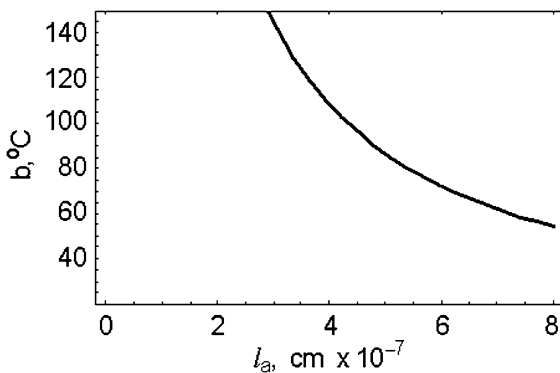

Fig. 5—Average site size, l_a, as a function of the b coefficient.

volume, and N_{Avo} is the Avogadro number. Accordingly, from Eqs. [11], [14], and [16], the average site sizes l_a can be given by

$$l_a = \frac{4T_e \gamma \sin \theta}{b} \left(\frac{V_m}{N_{Avo}}\right)^{1/3} \qquad [17]$$

Furthermore, for graphite nuclei, it can be assumed that $\gamma = 0.86$, $V_m = 5.45$ cm³/mol, $N_{Avo} = 6,024 \times 10^{23}$ mol⁻¹, $\theta = 25$ deg, and $T_e = 1427.1$ K. Plugging these data into Eq. [17], a relationship between l_a and the b coefficient is found that can be graphically plotted (Figure 5). Notice from this figure that the b coefficient decreases as l_a increases.

In addition, the $\Lambda(l)$ function describes the inherent amount and site sizes in the melt. Hence, using Eqs. [6], [15], and [17], the $\Lambda(l)$ function can be graphically plotted as shown in Figure 6. From Eqs. [10], [11], and [16] for $\Delta T = \Delta T_m = 20$ °C, $l_m = 2.16 \times 10^{-6}$ cm and sites of sizes greater than l_m become active. In the case of $N_s = 4.24 \times 10^7$ cm⁻³, $b = 20$ °C, and for $N_s = 4.01 \times 10^7$ cm⁻³, $b = 42$ °C; the number of active sites for nucleation sites becomes 1.55×10^7 cm⁻³ and 4.91×10^6 cm⁻³, respectively; they are shown by the shaded fields below the $\Lambda(l)$ curves in Figure 6, as estimated from Eq. [12], and are the same as predicted by Eq. [13].

III. EXPERIMENTAL PROCEDURE

The proposed model was experimentally corroborated for the case of ductile and flake graphite cast iron.
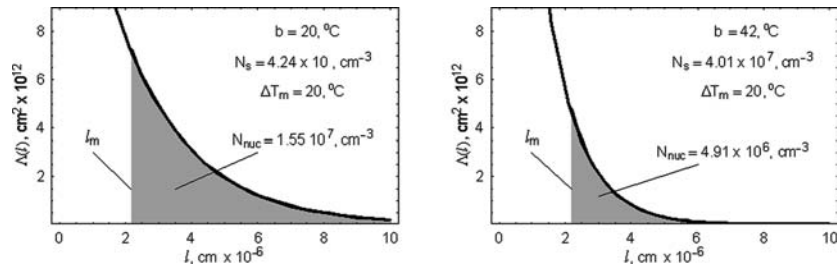
Fig. 6—Distribution functions for substrates in various melts with different physical-chemical states. The shaded fields under the $\Lambda(l)$ curves indicate the number of active nucleation sites.

Table I. Metallurgical Treatments Including Inoculants and Type of Spheroidizing Agents

No of Melt	Type of Metallurgical Treatment	Consumption, %, Type of Spheroidizer	Consumption, %, Type of Inoculants
1	Cast iron poured into mold after 4 min from inoculation (ladle)	0.91 K102	0.28 Zircinoc
2	Inoculation under down-gate	1.0 INJECTALLOY	0.28; Foundrysil
3	Double inoculation (ladle and pouring basin)	0.87 K102	0.87 Zircinoc + 0,3 RZM55AV
4	Inoculation in pouring basin	1.08 INJECTALLOY	0.65 Zircinoc
5	Inoculation in pouring basin	0.94 INJECTALLOY	1.0 FeSi75
6	Inoculation in pouring basin	0.8 PEM	0.55 RZM 55AV

Zircinoc: 73 to 75 pct Si; 1.0 to 2.5 pct Ca; 1.3 to 1.8 pct Zr; 1.0 to 1.5 pct Al Foundrysil: 73 to 79 pct Si; 0.75 to 1.25 pct Ca; 0.75 to 1.25 pct Ba; 0.75 to 1.25 pct Al RZM55AV: 63 to 67 pct Si; 1.0 to 2.0 pct Ca; 4.5 to 5.5 pct Zr; 1.5 to 2.0 pct Al FeSi 75: 75 pct Si; 1.0 to 1.2 pct Ca; 1.5 to 2.5 pct Al INJECTALLOY: 36 pct Si; 25 pct Mg; 3 pct Re PEM and K102—spheroidizers made by Pechiney, France

A. Ductile Cast Iron

In this case, the experimental melts were made in a low frequency (50 Hz) induction furnace of 8000-kg capacity. The raw materials employed were iron scrap, steel scrap, and ferrosilicon alloys. After melting and preheating at 1485 °C, molten iron was poured into a casting ladle where the spheroidization treatment was implemented using the cored wired injection method. Different inoculants in various amounts were used (Table I) in order to promote various degrees of maximum undercooling. The chemical composition of the experimental nodular cast irons is given in Table II.

The molten cast iron was poured into 6-, 10-, and 16-mm-thick plate molds of 100 mm in length and into 22-mm-thick plates of 140 mm in length. All of the plates had a common gating system. The casting molds were made from quick-hardening molding sand and they were instrumented with Pt/PtRh10 thermocouples in quartz sleeves of 1.6-mm diameter for 6- and 10-mm-thick plates. Quartz sleeves of 3-mm diameter were used for plates of other thicknesses. The thermocouple terminals (Pt/PtRh10) were placed at the geometrical center of each mold cavity, normal to the heat-transfer direction, in order to improve the measurement accuracy. From the experimental cooling curves (Figure 7(a)), the minimum temperature T_m, at the onset of eutectic solidification, was determined and hence the maximum undercooling for individual plates established using

Table II. Chemical Composition of Ductile Cast Iron

No of Melt	Chemical Composition (% Wt)					
	C	P	S	Si	Mn	Mg
1	3.62	0.02	0.02	2.68	0.51	0.05
2	3.73	0.01	0.02	2.57	0.43	0.04
3	3.62	0.01	0.02	2.65	0.44	0.03
4	3.71	0.02	0.01	2.77	0.44	0.04
5	3.75	0.03	0.01	2.77	0.42	0.03
6	3.61	0.02	0.01	2.67	0.51	0.04

$$\Delta T_m = T_e - T_m$$

where

$$T_e = 1153.9 + 5.25Si - 14.88P \qquad [19]$$

In the preceding expression, T_e is the stable equilibrium temperature of the graphite eutectic[2] and Si, and P are the carbon, silicon, and phosphorus contents in cast iron, respectively.

Metallographic evaluations of nodule counts were made on samples cut from the plate geometrical centers. Figure 8(a) shows a typical nodule structure found in melt 6. The area nodule count, $N_{A,n}$ (number of graphite nodule per unit area of metal), was measured using a Leica Q Win quantitative analyzer. In ductile iron, the graphite nodule was characterized by a Raleigh distribution.[24] Accordingly, the volumetric nodule count, $N_{V,n}$, was estimated from $N_{A,n}$ using the Wiencek expression:[25]
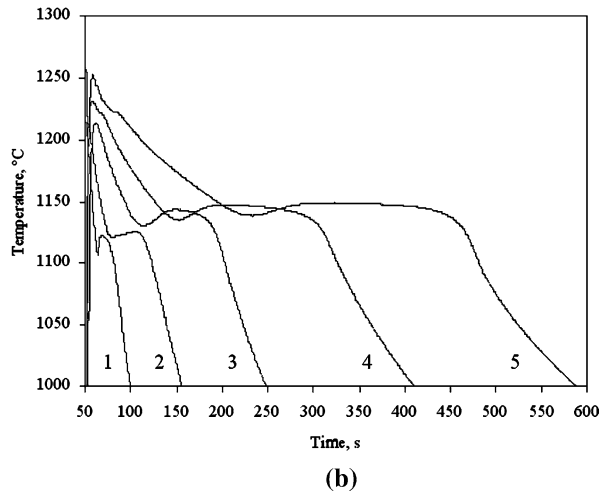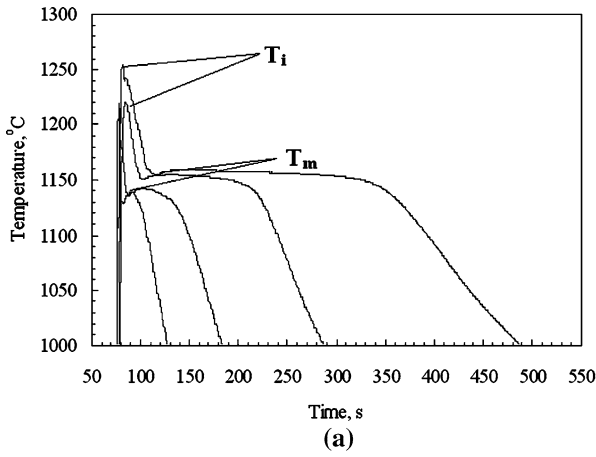
Fig. 7—Cooling curves for (a) ductile and (b) flake cast iron of different wall thicknesses.

$$N_{V,n} = \sqrt{\frac{N_{A,n}^3}{g_{gr}}}$$

where g_{gr} is the volumetric fraction of graphite, with $g_{gr} \approx 0.12$ at room temperature.
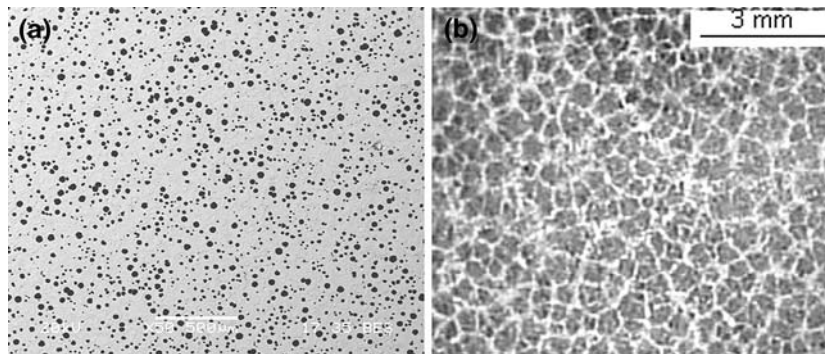
Table III. Inoculation Times and Exhibited Chemistry in Flake Graphite Cast Irons

No of Castings	Time after Inoculation, Min	Chemical Composition, Wt. Pct				
		C	Si	Mn	P	S
I/1	1.5	3.14	1.98	0.13	0.091	0.067
I/2	5	3.18	2.05	0.11	0.093	0.061
I/3	10	3.16	2.04	0.13	0.095	0.065
I/4	15	3.21	2.01	0.14	0.095	0.053
I/5	20	3.20	2.08	0.13	0.098	0.050
I/6	25	3.16	2.08	0.13	0.091	0.052

B. Flake Graphite Cast Iron

The experimental melts were made in an electric induction furnace of medium frequency and a 15-kg capacity crucible. The furnace charge materials were pig iron, steel scrap, commercially pure silicon, sulphur, and ferrophosphorus. After melting and preheating at 1420°C, the liquid iron was inoculated using Foundrysil (73 to 75 pct Si, 0.75 pct Al, 0.75 to 1.25 pct Ca, and 0.75 to 1.25 pct Ba) with a 2- to 5-mm granulation added as a 0.5 pct of the charge weight. Samples of inoculated iron were taken at various successive time intervals of 1.5, 5, 10, 15, 20, and 25 minutes from the instant of inoculation. In this case, the cast iron was poured into foundry molds similar to the ones used in ductile iron (i.e., instrumented with thermocouples). In addition, samples were cast for chemical analyses. Table III shows the experimental data on times after inoculation and the chemical composition of the cast iron. Figure 7(b) shows the exhibited cooling curves after 25 minutes from inoculation as a function of the wall thickness.

The metallographic characterization consisted of sample polishing and then etching with Stead reagent to reveal the cell boundaries. Figure 8(b) shows the typical microstructure (on the specimen cross section) of eutectic cell boundaries found in cast iron after 25 minutes of inoculation. The area cell count N_A (number of cells per unit area of metal) was determined using the so-called variant II of the Jeffries method, which after applying the Saltykov formula can be written as[26,27]

Fig. 8—(a) Exhibited graphite nodule structure and (b) cell boundaries in graphite eutectic, etchant: Stead reagent.

Table IV. Experimental Results for Ductile Iron

Number	Wall Thickness s, mm	Undercooling ΔT_m, °C	Nodule Count $N_{A,n}$, mm^{-2}
1	6	45	270
	10	36	150
	16	21	106
	22	18	104
2	6	49	327
	10	34	224
	16	26	130
	22	20	127
3	6	43	313
	10	33	224
	16	21	135
	22	13	118
4	6	35	400
	10	24	305
	16	15	252
	22	10	150
5	6	30	440
	10	22	337
	16	12	264
	22	10	143
6	6	41	336
	10	31	221
	16	19	155
	22	16	120

Table V. Experimental Results for Flake Graphite Cast Iron

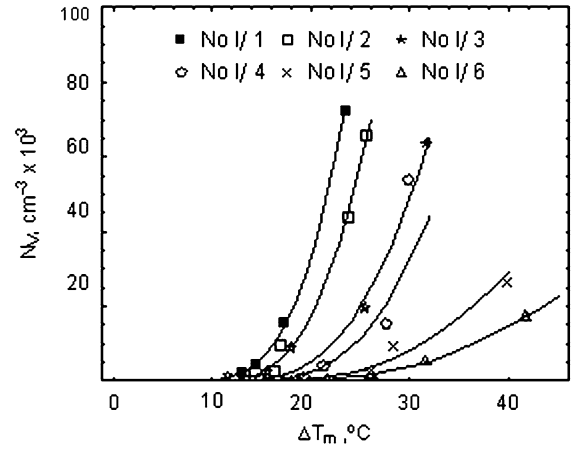| No of Casting Time after Inoculation, t_i— Absolute t—Relative	Wall Thickness s, mm	Cell Count N_A, cm^{-2}	Maximum Undercooling Measured ΔT_m, °C
I/1 $t_i = 1.5$	10	2480	23.4
min $t = 0.06$	16	893	17.2
	22	337	14.2
	30	226	12.7
I/2 $t_i = 5$	6	2319	25.5
min $t = 0.20$	10	1773	23.7
	16	654	15.8
	22	256	16.3
	30	185	13.1
I/3 $t_i = 10$	6	2277	31.5
min $t = 0.40$	10	1043	25.4
	16	612	16.8
	22	264	15.4
	30	170	11.4
I/4 $t_i = 15$	6	2036	29.8
min $t = 0.60$	10	880	27.6
	16	364	20.3
	22	132	19.3
	30	59	14.5
I/5 $t_i = 20$	6	1270	39.6
min $t = 0.80$	10	638	28.0
	16	176	25.7
	22	94	18.8
	30	52	17.5
I/6 $t_i = t_f = 25$	6	950	41.4
min $t = 1.0$	10	437	31.4
	16	175	25.8
	22	84	21.5
	30	47	18.5

Fig. 9—Plots of volumetric eutectic cell count *vs* maximum degree of undercooling.

$$N_A = \frac{N_i + 0.5N_c + 1}{A}$$

where N_i is the number of cells inside a rectangle W, N_c is the number of cells that intersect a W side but not its corners, and A is the surface area of W. The graphite eutectic exhibits a granular microstructure (Figure 8(b)). Hence, as a first approximation, it may be assumed that the spatial cell configurations follow the so-called Poisson–Voronoi model. Then, the stereological formula given subsequently[28] for cell density N_V can be employed in this work:

$$N_V = 0.5680(N_A)^{3/2} \qquad [22]$$

IV. RESULTS AND DISCUSSION

Tables IV and V show the experimental results for the measurements of maximum degree of undercooling, ΔT_m, as well as nodule $N_{A,n}$ and cell N_A counts for melts I/1 through I/6 and 1 through 6. From these results, it
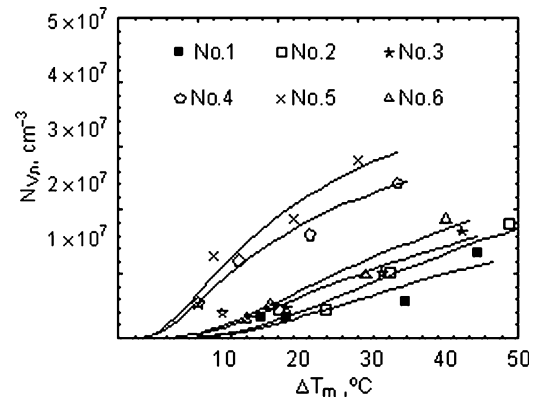

Fig. 10—Volumetric nodule count *vs* maximum degree of undercooling.

Table VI. Correlation and Nucleation Coefficients

| | Flake Graphite Cast Iron | | | | Ductile Cast Iron | | |
| | | Nucleation Coefficients | | | | Nucleation Coefficients | |
Number	Correlation Coefficients	$N_s(cm^{-3})$	$b(°C)$	Number	Correlation Coefficients	$N_s(cm^{-3})$	$b(°C)$
I/1	0.99	$6.1 \cdot 10^6$	104	1	0.88	$4.13 \cdot 10^7$	58
I/2	0.99	$6.8 \cdot 10^6$	119	2	0.98	$5.69 \cdot 10^7$	60
I/3	0.99	$4.4 \cdot 10^6$	135	3	0.96	$4.01 \cdot 10^7$	42
I/4	0.86	$5.4 \cdot 10^6$	154	4	0.98	$4.24 \cdot 10^7$	20
I/5	0.98	$1.3 \cdot 10^6$	152	5	0.96	$5.16 \cdot 10^7$	20
I/6	0.99	$8.4 \cdot 10^5$	162	6	0.97	$4.85 \cdot 10^7$	43
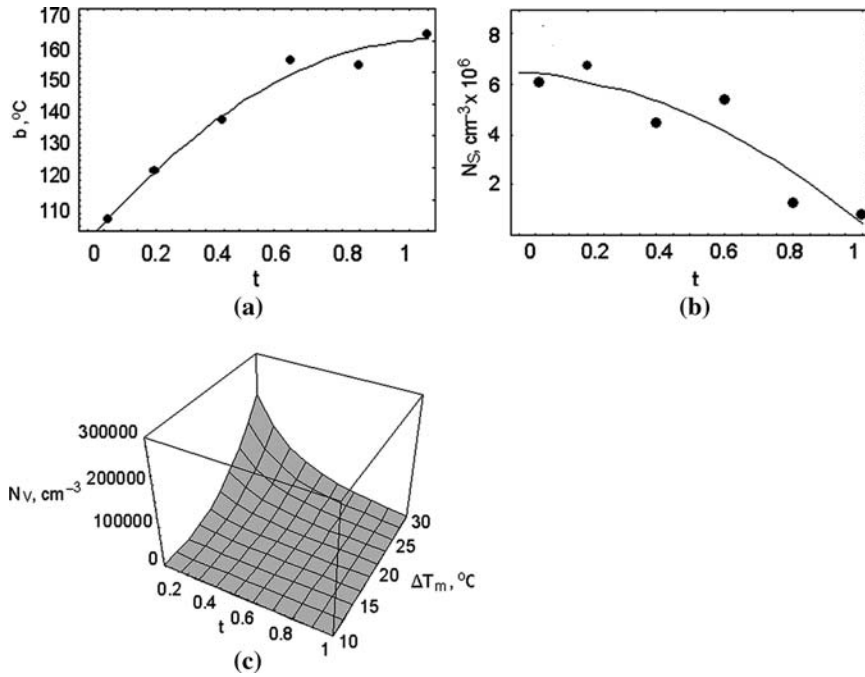
Fig. 11—Effect of dimensionless time t after inoculation on the nucleation coefficients (*a*) b and (*b*) N_s and eutectic cell count N_V vs maximum degree of undercooling ΔT_m and (*c*) of dimensionless time t.
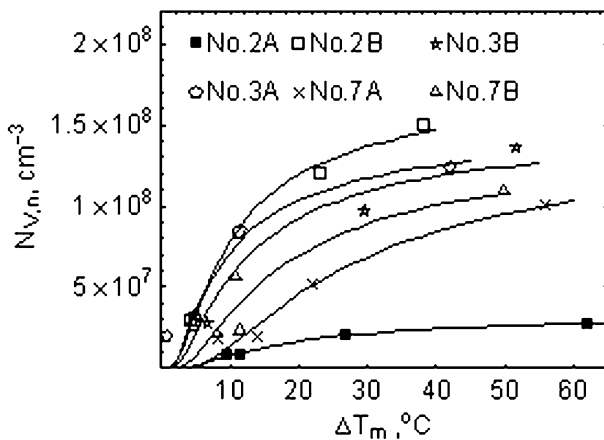

Fig. 12—Volumetric nodule count *vs* maximum degree of undercooling for castings 2A through 7B.

can be inferred that for a given melt, as the wall thickness, s, of the casting increases, ΔT_m decreases, and hence the nodule or cell count decreases.

Considering the experimental ΔT_m, $N_{A,n}$, and N_A values for a given melt, correlation expressions were derived. These expressions are plotted in Figures 9 and 10, and the nucleation coefficients, N_s and b (which determine the respective melt nucleation susceptibilities for graphite), are given in Table VI. In these calculations, the correlation coefficients are relatively high (Table VI), suggesting that in each case, the relationships between N_V, $N_{V,n}$, and ΔT_m described by Eq. [13] are in good agreement with the experimental outcome.

The experimental results from Figures 9 and 10, as well as the correlation curves for cast irons from different melts, strongly suggest that each cast iron is characterized by a given physical-chemical state
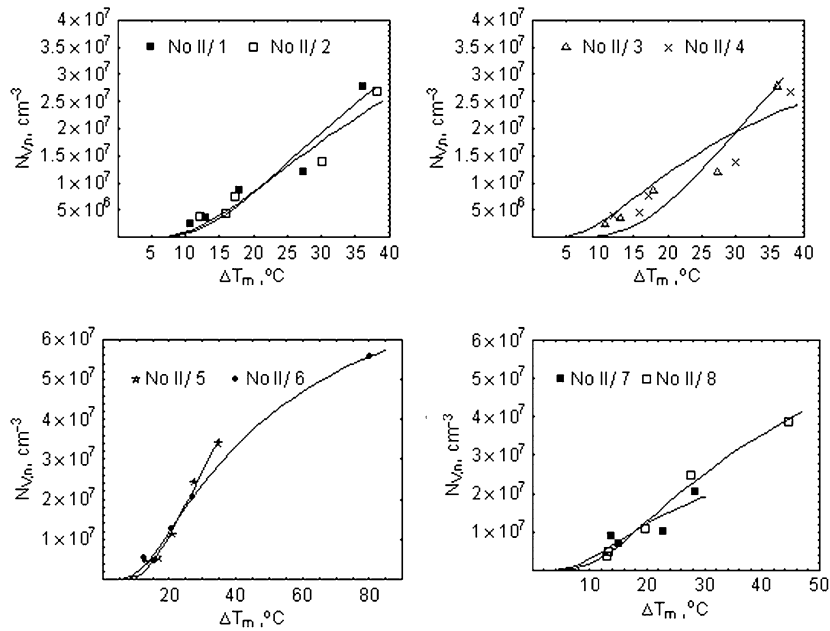
Fig. 13—Volumetric nodule count *vs* maximum degree of undercooling for melts 1–8.

Table VII. Nucleation Coefficients

Number	Nucleation Coefficients		Number	Nucleation Coefficients	
	N_s cm^{-3}	b °C		N_s cm^{-3}	b °C
2A	$3.55 \cdot 10^7$	15.43	II/1	$1.05 \cdot 10^8$	51
2B	$1.80 \cdot 10^8$	8.24	II/2	$7.94 \cdot 10^7$	45
3A	$1.51 \cdot 10^8$	9.80	II/3	$5.26 \cdot 10^7$	30
3B	$1.50 \cdot 10^8$	7.36	II/4	$1.74 \cdot 10^8$	66
7A	$1.55 \cdot 10^8$	24.55	II/5	$1.62 \cdot 10^8$	54
7B	$1.45 \cdot 10^8$	14.73	II/6	$9.31 \cdot 10^7$	41
—	—	—	II/7	$4.88 \cdot 10^7$	28
—	—	—	II/8	$9.86 \cdot 10^7$	41

2A, 2B—C = 3.76 pct; Si = 2.39 pct 3A, 3B—C = 3.79 pct; Si = 2.60 pct 7A, 7B—C = 3.66 pct; Si = 2.55 pct II/1 to II/4—C = 3.66 pct; Si = 2.40 pct; P = 0.012 pct II/5 to II/8—C = 3.72 pct; Si = 2.38 pct; P = 0.011 pct
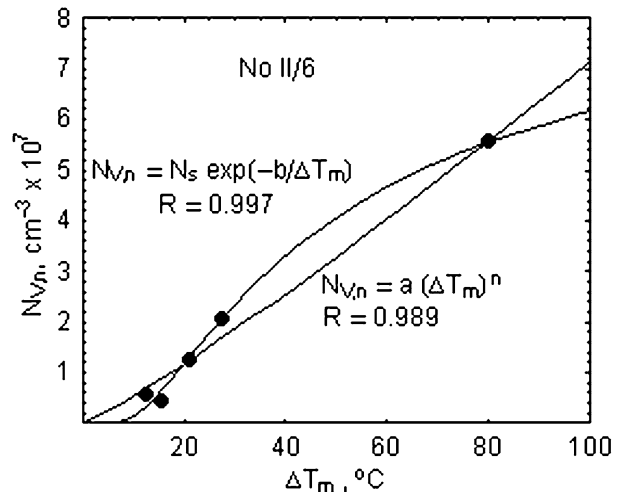

Fig. 14—Results of calculations according to Eqs. [1] and [13] for melt II/6, $N_s = 9.31 \cdot 10^7$ cm^{-3}, b = 41.3755 °C, $a = 0.0406$ cm^{-3}/°C^n, and $n = 1.1236$.

(induced by different metallurgical treatment of the liquid metal). Hence, it is not surprising to find different nucleation coefficients, N_s and b, for the various cast irons. Yet, in each case, a relationship between ΔT_m and cell N_V or nodule count $N_{V,n}$ (Eq. [13]) is found.

From Table V, it is evident that the inoculation effect expressed in terms of cell count depends on ΔT_m and that it is a function of the time t_i counted from the instant of metal bath inoculation. After 25 minutes from the onset of inoculation, the changes in cell count are negligible, and this time can be considered as a reference point. Accordingly, any cell count changes can be correlated to the dimensionless time

$$t = \frac{t_i}{t_f}$$

where t_i is the time from the instant of metal bath inoculation and t_f is the time beyond which total fading of the inoculation effect is observed. From Tables V and VI, it can be observed that N_s and b in Eq. [13] are time dependant. Figure 11 shows the dependence of N_s and b as a function of the dimensionless time t. Using a polynomial approximation, regression expressions can be found, which can be described by
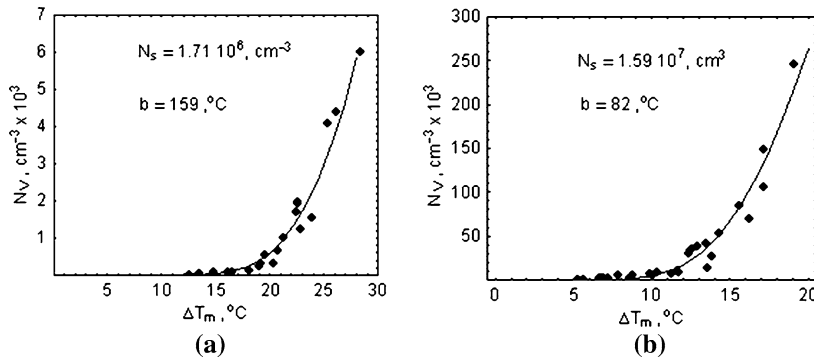
Fig. 15—Plots of volumetric eutectic cell count *vs* maximum degree of undercooling: (*a*) uninoculated and (*b*) inoculated cast iron.

$$b = 96.9 + 122.6\, t - 59.2\, t^2 \qquad [24]$$

$$N_s = 10^6 \left(6.5 - 0.8t - 5.3t^2\right) \qquad [25]$$

Considering Eqs. [13], [24], and [25], an expression can be found for the cell count N_V as a function of ΔT_m and t after inoculation as

$$N_V(t) = N_s(t) \exp\left[-\frac{b(t)}{\Delta T_m}\right] \qquad [26]$$

where $N_s(t)$ and $b(t)$ are given by Eqs. [24] and [25], respectively.

From Eqs. [24] through [26], it is apparent that at increasing ΔT_m (decreasing wall thickness s), N_V increases, while prolonged times, t, after inoculation have an opposite effect (Figure 11(c)).

It is worth noting the work of Lesoult *et al.*[29] and Wessen *et al.*,[30] who used cast iron after different metallurgical treatments and who estimated the ΔT_m and nodule count $N_{V,n}$. The points in Figures 12 and 13 show the results of these experimental results. The values of coefficients N_s and b can be estimated similarly as before and are given in Table VII. The correlation coefficients R for relationships given in Figures 12 and 13 are high and are situated in the range of 0.93 to 0.99. Figure 14 shows the results of calculations for melt II/6 according to Eqs. [1] and [13]. It is worth pointing out that in a wide range of undercooling, Eq. [13] has better matching to experimental results ($R = 0.997$) than Eq. [1], where $R = 0.989$. Moreover, Oldfield's empirical Eq. [1] is a concave function, which approaches infinity, while Eq. [13] is a convex function, which approaches $N_s = \text{const.}$

It is also interesting to present experimental results (Figure 15) of an extended investigation made by Mamapaey[31] between the eutectic cell count in uninoculated and inoculated flake graphite cast iron and a rather small range of undercooling ΔT_m. Once again the correlation coefficients of relationships given in Figure 15 are high, ≈ 0.98.

From Tables VI and VII, for the different melts (different chemical composition and different type of metallurgical treatment and in consequence for liquid with different the substrate nucleation size distribution), the fact that nucleation coefficients N_s and b for a given melt are different from each other is not surprising. However, in each case and independent from the authors of the experiments, it can be stated that N_V and $N_{V,n}$ are exponential functions of ΔT_m, and it is evident that they can be described by analytical Eq. [13], thus confirming that the proposed theory is in good agreement with the experimental evidence.

V. CONCLUSIONS

1 In this work, a theory is proposed that relates the density of nuclei, and hence the graphite nodule and eutectic cell count, with the maximum degree of undercooling. This theoretical analysis is experimentally verified.
2 It has been shown that the nodule and eutectic cell count in cast iron can be described by an exponential expression, which is a function of the maximum undercooling, ΔT_m, and of the parameters N_s and b. In particular, the experimental evidence strongly suggests that N_s and b are functions of the physical-chemical state of the liquid cast iron.
3 The proposed theory provides a physical interpretation for the nucleation constants found in empirical expressions used in the literature to account for the nucleation stage during solidification.

REFERENCES

1. E. Fraś and C. Podrzucki: *Inoculated Cast Iron*, AGH, Cracow, 1978.
2. E. Fraś and H.F. Lopez: *Acta Metall. Mater.*, 1993, vol. 41, pp. 3575–83.
3. E. Fraś and H.F. Lopez: *AFS Trans.*, 1994, vol. 102, pp. 597–601.

4. H. Morrogh: *J. Iron Steel Inst.*, 1968, pp. 1–10.
5. J. Liu and R. Elliot: *Int. J. Cast Met. Res.*, 1999, vol. 11, pp. 407–12.
6. H.J. Heine: *Foundry Management Technol.*, 1988, pp. 20–23.
7. M.N. Achmadabadi, N. Niyama, and T. Ohide: *AFS Trans.*, 1994, vol. 102, pp. 269–78.
8. A. Javaid, J. Thompson, and K.G. Davis: *AFS Trans.*, 2002, vol. 110, pp. 889–98.
9. A. Javaid, J. Thompson, M. Sahoo, and K.G. Davis: *AFS Trans.*, 1999, vol. 107, pp. 441–56.
10. V. Venugopalan: *Metall. Trans. A*, 1990, vol. 21A, pp. 913–18.
11. R.E. Ruxanda, D.M. Stefanescu, and T.S. Piwonka: *AFS Trans.*, 2002, vol. 110, pp. 1131–47.
12. H.D. Merchant: *Recent Research on Cast Iron*, Gordon and Breach Science Publishers, New York, NY, 1968 100.
13. E. Fraś, T. Serrano, and A. Bustos: *Fundiciones de Hierro*, ILAFA, Chile, 1990.
14. M.E. Henderson: *Ductile Iron Handbook*, AFS, Des Plaines, 1992, pp. 167–176.
15. X. Guo: *Int. J. Cast Met. Res.*, 2003, vol. 16(1–3), pp. 17–22.
16. D.M. Stefanescu: *Physical Metallurgy of Cast Iron V*, Scitec Publication, Zurich, 1997, pp. 89–104.
17. E. Fraś, W. Kapturkiewicz, and H.F. Lopez: *AFS Trans.*, 1992, vol. 100, pp. 583–91.
18. H. Fredriksson and U. Akerlind: *Materials Processing during Casting*, John Wiley & Sons, Ltd, Chichester, England, 2006.
19. W.A. Oldfield: *Trans. ASM*, 1966, vol. 59, pp. 945–61.
20. D.M. Stefanescu: *Science and Engineering of Casting Solidification*, Kluwer Academic/Plenum Publishers, New York, NY, 2002.
21. G. Lesoult, M. Castro, and J. Lacaze: *Acta Mater.*, 1988, vol. 46(3), pp. 983–95.
22. W.T. Eadie, D. Drijard, F.E. James, M. Roos, and B. Sadoulet: *Statistical Methods in Experimental Physics*, North-Holland, London, 1982.
23. C.V. Thompson and F. Spaepen: *Acta Metall.*, 1983, vol. 31, pp. 2021–27.
24. L. Wojnar: *Acta Stereologica*, 1986, vol. 5/2, pp. 319–24.
25. K. Wiencek and J. Ryś: *Mater. Eng.*, 1998, vol. 3, pp. 396–99.
26. J. Ryś: *Stereology of Materials*, Fotobit, Cracow, 1995.
27. D. Stoyan, W.S. Kendall, and J. Mecke: *Stochastic Geometry and Its Application*, John Wiley & Sons, Chichester, 1995.
28. J. Ohser and U. Lorz: *Quantitative Gefuegeanalyse*, DVG Leipzig, Stuttgart, 1994.
29. G. Lesoult, M. Castro, and J. Lacaze: *Acta Mater.*, 1998, vol. 46, pp. 997–1010.
30. M. Wessen, I. Svensson, and R. Aagaard: *Int. J. Cast Met. Res.*, 1999, vol. 11, pp. 351–56.
31. F. Mamapaey: *55th Int. Foundry Congr.*, Moscow, 1988.